Available online at www.scientiaresearchlibrary.com

Scientia Research Library

ISSN 2348-0424
USA CODEN: JETRB4

Journal of Engineering And Technology Research, 2014, 2 (2):12-29
(*http://www.scientiaresearchlibrary.com/arhcive.php*)

Multi-parametric study of sizes of dielectric barrier discharge setup and its effects on engineering of low temperature plasma jets

N.Jomaa, M. Yousfi[1], O. Eichwald, N.Merbahi
Université Paul Sabatier, LAPLACE, UMR CNRS 5213[1]
118, route de Narbonne, 31062 Toulouse Cedex 9, France

ABSTRACT

This work is devoted to the optimization of a classical setup generating a low temperature plasma jet launched in open air by using helium flow carrier gas through a glass tube. The dielectric barrier discharge setup uses a tube wrapped by two thin cylindrical external electrodes powered by a mono-polar pulsed high voltage supply. The optimization is based on a multi-parameter study covering a wide range of the tube and electrode sizes and also the dielectric permittivity of the tube. The aim is to analyze individually the effect of each of these tube parameters on the magnitude of the geometric downstream electric field which is directly correlated to the efficiency of the dynamics of the generated ionization waves or "plasma bullets". Such correlations are shown by using fluid modeling of plasma jet dynamics and experimental measurements of discharge current and plasma jet length. Two distinct configurations of the plasma jet setup have been considered: a standard configuration and an experimental optimized one. The optimization of plasma jet characteristics has shown that for a fixed high voltage magnitude (5kV), the optimal jet length is reached for the lowest dielectric permittivity, the smallest downstream electrode width, the largest upstream electrode width, the thinnest electrode thickness, the smallest inter-electrode distance, the thinnest tube thickness and the smallest tube diameter. This allows us to suggest a theoretical optimal configuration that gives a maximum value of downstream electric field about 5 times higher than the standard case. This theoretical optimal configuration enables to design electric power supply using voltage about 5 times lower (1 kV) than the standard voltage (5kV)to generate the same low temperature plasma jet.

INTRODUCTION

Many research works have been already devoted to low temperature plasma jets enabling remote treatments outside of the plasma generation region and targeting mainly-but not only- the field of biomedical applications such as inactivation of plank tonic bacteria (see e.g. refs [1-2])or biofilms (see e.g. refs [3-4]), biomaterial treatment(see e.g. refs [5-7]) and medicine (see e.g. refs [8-13]). A special section in an international journal illustrates the growing interest of the scientific community on plasma jets and bullets; it is prefaced by Kong et al (see [14] and references given therein) that summarize the history on these kinds of plasmas, their variety and their diverse applications. The

reader can also find many other interesting works on plasma jets in the literature (see e.g. refs [15-36]).

The literature investigations on the low temperature plasma jets generated more particularly by a system of dielectric barrier discharge (DBD) along a quartz tube crossed by a helium carrier gas ,were generally aimed to better understand the hydrodynamics, the ionizing wave (or bullet)dynamics and the chemical properties. The targeted objectives are generally to better control for instance the produced active species and the jet temperature versus the complex and numerous set of operating parameters (gas composition and flow, applied voltage, size and nature of dielectric tube, size and position of electrodes, etc.) in order to tune such plasmas towards each specific biomedical application. These literature investigations based on experimental analyses (see e.g. [15-33]) and also on a few recent works on modeling and simulation(see e.g. [34-36]) have already given a lot of very interesting results with, in some cases, the variation of operating parameters as for instance the gas composition including additive [27], the gas flow rate ([20] or [22] or [25]), the nature of inlet gas [28], the power supply characteristics ([20], [22-23], [29-31]), the electrode configuration([21], [31-33]), etc.

The present work presents a different parametric study. It is devoted to a multi-parametric analysis based on a wide variation of the geometric sizes of the tube and the electrodes and also on the variation of the nature of dielectric tube used in the case of the considered standard helium DBD plasma jet. The aim of this study is to help to design electric power supply using voltage lower than the standard power supply to generate the same low temperature plasma jet.

To reach this aim, this study is more particularly based on 2D*r,z*electric field calculations in the case of each considered set of operating parameters. The aim is to obtain, for fixed parameters of the power supply and carrier gas velocity, the optimal geometric parameters allowing the optimal plasma characteristics at a given position on the axis outside the dielectric tube. The plasma characteristics can correspond for instance to the longest jet length, the highest plasma bullet velocity and the largest electron density or electric field at a fixed position on the axis in the downstream side. The fixed position can correspond for instance to the position (e.g. 1 cm from the tube exit) where a living tissue can be placed for plasma exposure. The trends determined from such geometric electric field calculations are then confirmed from both experimental measurements and fluid modeling of ionizing wave (or plasma bullet) dynamics. Section 2 following this introduction is devoted to the method of the electric field calculation that directly affects the plasma characteristics such as the length of the plasma jet and the magnitudes of electron density and electric field at a fixed position outside the tube in ambient air. Then section 3 displays the obtained results with a discussion on their experimental and modeling confirmations. A comparison has been done more particularly between a reference (or standard) case using classical sizes of the quartz tube and electrodes and an optimized case. The latter is based on the choice of a set of experimentally possible operating parameters that gives the optimal jet length and plasma characteristics outside the tube in the downstream side outside the dielectric tube.

MATERIALS AND METHODS

Formalism and method of calculation:

The configuration of the quartz tube crossed by helium gas flow, wrapped by two electrodes (powered and grounded ones)and powered by a pulsed voltage supply is shown in figure 1a.The position of the powered electrode is chosen on the downstream side.

Figure 1b displays the geometric configuration with the different variable parameters corresponding to the sizes of the tube and the electrodes.

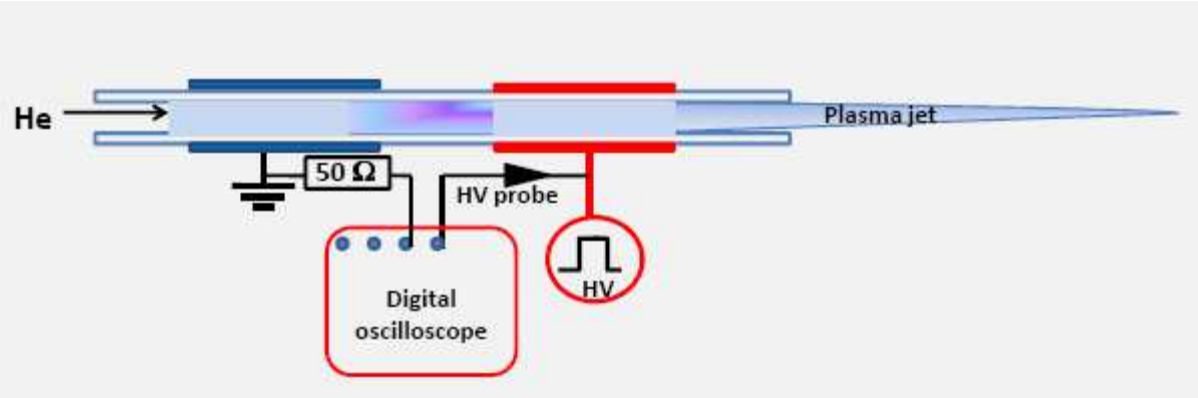

Figure 1a: Schematic representation of the DBD setup generating the low temperature plasma jet

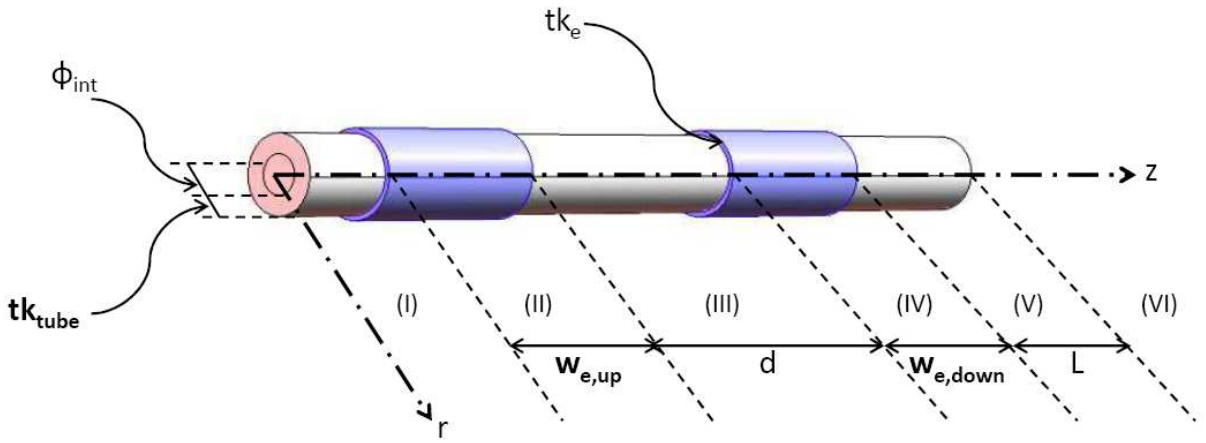

Figure 1b: Dielectric tube used to generate helium DBD plasma jet with the different geometric parameters as ϕ_{int} (internal diameter of the tube), tk_{tube}(thickness of the tube), $w_{e,up}$ (width of the upstream electrode or grounded electrode), $w_{e,down}$ (width of the downstream electrode or powered electrode), d (inter-electrode distance), tk_e (thickness of the electrode) and L (length of the tube on the downstream side).The different regions along the tube axis are numbered from (I) to (VI).

The space variation of the electric field in air and in dielectric material in the case of cylindrical *(r,z)*geometry having a revolution symmetry around z axis is obtained from the solution of the following equation:

$$\frac{1}{r}\frac{\partial \varepsilon_0 \varepsilon_r r E_r}{\partial r} + \frac{\partial \varepsilon_0 \varepsilon_r E_z}{\partial z} = \rho_V \qquad (1)$$

E_r and E_z are the radial and axial components of electric field vector $\boldsymbol{E}$.ε_0 isthe dielectric permittivity of vacuum and ε_r the relative permittivity of the dielectric material (either glass tube or air) while $\rho_V$is the space charge distribution.

The fluid model used for the simulation of the formation and the propagation of ionizing waves (or bullets) is based on the classical conservation equations of charged particles (electrons and ions) coupled to Maxwell-Gauss equation (1) for the calculation of the charge space electric field. The details on numerical method of solution of the different equations of the present fluid model have been already detailed elsewhere [36]with the basic data needed for the considered interactions between charged particles (electrons and ions) and helium background gas (inside the tube) and helium/air mixtures (outside the tube). A particular emphasis was done in ref [36] on specific

interactions contributing either to increase the electron avalanches (as direct and stepwise ionizations) or to propagate the ionization waves (as Penning ionization) during the electrical discharge development.

RESULT AND DISCUSSION

A standard (or reference) case has been first chosen for the calculations of the geometric or initial electric field (section 3.1), the simulation of discharge dynamics (section 3.2) and the experimental measurements of the discharge current and the plasma jet length (section 3.3). A quartz tube (ε_r=4.2) is used in the standard case with internal diameter ϕ_{int}=2mm, tube thickness tk_{tube}=1mm, width of the upstream electrode $w_{e,up}$=20mm, width of the downstream electrode $w_{e,down}$=20mm, inter-electrode distance *d*=10mm, thickness of the electrode tk_e=0.2mm and tube length on the downstream side L=10mm.

Calculations of the geometric or initial field along the tube axis:

The geometric or initial electric field is calculated from numerical solution of equation (1) without considering the space charge in order to know exactly the shape and the magnitude of the initial electric field acting or accelerating the charged particles as soon as a high voltage is applied to the powered electrode (downstream one in our case). It is noteworthy that such electric field ,that depends only on the geometry of the tube device, is determined without taking into account the space charge by considering ρ_V=0 in equation (1).

The aim is first to show the more or less strong dependence of this initial electric field on the different parameters of the tube geometry defined in figure 1b. Then in the following sections, it is shown how this initial field affects the plasma jet characteristics such as simulated space charge electric fields or electron density (section 3.2) and measured discharge current and jet length (section 3.3).

Figure 2 shows, in the standard case ,the geometric reduced electric field along the tube axis from z=0 up to a maximum position z=140 mm situated outside the quartz tube having a total length of 90 mm. The geometric electric field described in figure 2 in the standard case is generated by the potential displayed in figure 3 where a high voltage of 5kV is applied to the powered electrode placed in this case on the downstream side.

Calculations and also measurements in the present work are done in the case of atmospheric pressure at ambient temperature which corresponds to a background gas density N equal to 2.4457×10^{19} cm^{-3}.Before to describe the discharge behavior at the end of this section ,it should be noted:

-The symmetric shape and the relatively high magnitude of the electric field in the gap space(region III) between the two electrodes (from z=50mm to z=60mm): it is the initial electric field that enables to the dielectric barrier discharge to be ignited inside the quartz tube in pure helium within the gap space when the pulsed high voltage is applied. In fact, region III corresponds to the inter-electrode gap where there are complex discharge dynamics. This discharge dynamics already were evoked elsewhere[36]. In short, as soon as the high voltage is applied to the powered electrode, two discharges are initiated in region III from the high electric field zones (corresponding to the two electric field peaks shown in region III of figure 2). From each electric field peak of region III, two discharges are simultaneously started along z axis: one discharge propagating towards the left direction and one propagating towards the right direction. The two discharges propagating inwards the center of region III lead to the formation of plasma region with a very low electric field due to high concentration of both positive and negative charged particles. The two other discharges propagate in the opposite direction i.e. from region III to respectively region II and IV. In fact,

when the pulsed voltage is applied, two discharges were started simultaneously in an opposite direction along z axis from each electric field peak (i.e. high electric field zone). This means that each of the four electric field peaks (higher than 10Td) displayed in figure 2 is the starting-point of two discharges. If for instance, we follow the discharge propagating toward region IV. A plasma zone is reached in region IV where the electric field becomes very low before the starting of the ionizing wave dynamics from the peak of the initial electric field of region V. Therefore, this high geometric electric field in region V generates the dynamics of the plasma bullets that are launched in open air outside the dielectric tube as discussed in section 3.2. Last, between two successive pulsed voltages, the charged particles and the long lived excited species formed in the plasma region III are transported in region V and VI due to the flowing gas. The presence of such background species allow the plasma bullets (or ionizing waves) to propagate inside a pre-ionized and pre-excited gas medium favoring for instance Penning and stepwise ionizations necessary for the discharge development outside the tube and largely discussed in ref 36.

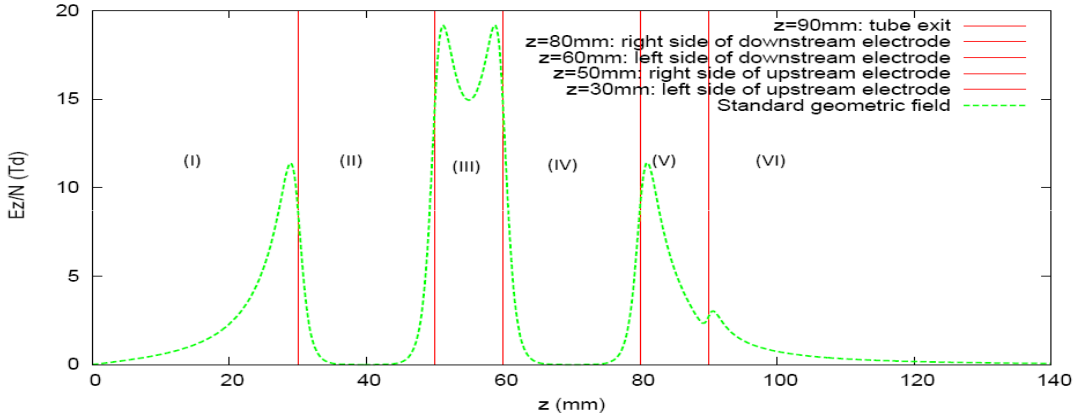

Figure 2:Modulus of standard geometric reduced electric field along the z axis (radial position r being equal to 0) for a high voltage of 5 kV applied to the powered electrode (placed between z=80mm to z=90 mm) in the standard case with a quartz tube of 90 mm for total length.

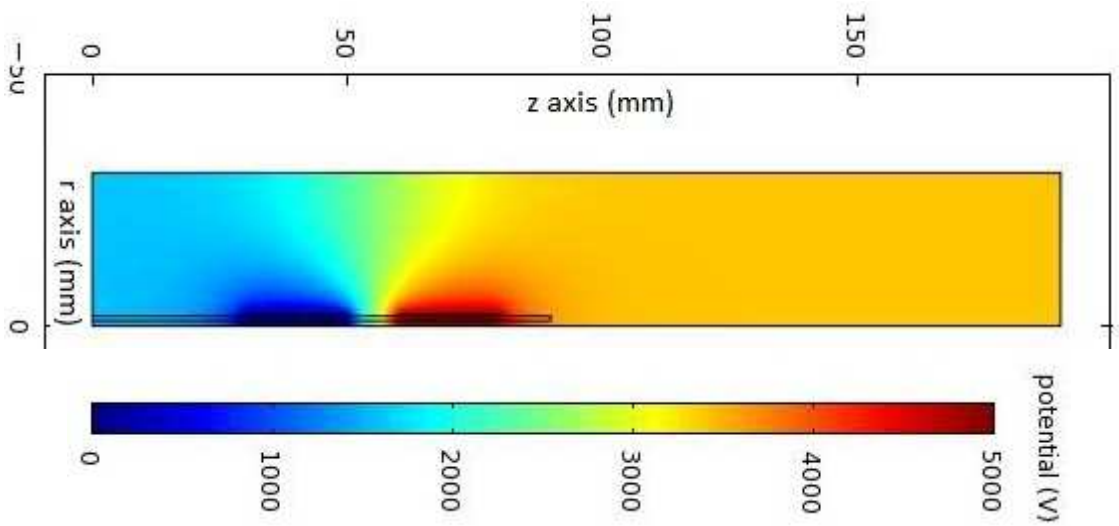

Figure 3: Potential distribution in the standard case with 5 kV applied to the powered electrode placed on the downstream side (surrounded by dark red color) in front of the upstream grounded electrode (surrounded by dark blue color).

- The shape and the magnitude of the electric field in region I between the tube input (z=0mm) and the left side of upstream electrode (z=30mm): it is the electric field in addition to the space charge one that generates

the ionization waves (usually experimentally observed) moving in the opposite direction of the gas flow (in the upstream side) inside the tube of gas injection.

- The shape with two peaks of the electric field generated in regions V and VI in the downstream side between z=80mm (right border of downstream electrode) to z=140mm (placed outside the glass tube): it is the electric field in addition with the corresponding space charge one that generates the ionizing waves launched on the downstream side and analyzed in the present work. The second peak observed at z=90mm (exit of the tube) is due to the change of dielectric permittivity between quartz and gas. It should be also noted that the maximum value of the downstream electric field (for z near 80mm) is quasi-equivalent to the upstream field maximum (for z near 30mm).

In fact, the magnitude of the electric field in regions V and VI of the downstream side (for $z \geq 80$ mm) has a direct effect on the properties of the ionization waves ejected outside the tube in the downstream side.

Before to show the correlation between the magnitude of the downstream electric field (for $z \geq 80$ mm) and the plasma jet characteristics(jet length, electron density, space charge electric field, discharge current) , we give in the following a multi-parametric study showing the effects of variation of the geometry and nature of the tube and the electrode sizes and position on the magnitude and the shape of the initial geometric field.

Effect of tube and electrode parameters on geometric electric field

The control configuration corresponds to the standard case of the plasma jet device with a given set of operating parameters (internal diameter of the tube=2mm, thickness of the tube=1mm, width of the upstream electrode=20mm, width of the downstream electrode=20mm, inter-electrode distance=10mm, electrode thickness=0.2mm and relative dielectric permittivity of the tube=4.2). Then for the multi-parametric study, each parameter has been separately changed. The aim is to show the effect of each parameter on the shape and the magnitude of the geometric downstream electric field which plays a central role on the characteristics of the plasma jet.

Figure 4 displays the downstream geometric field in regions IV to VI($z \geq 70$ mm)in the case of 3 values of the tube thickness (0.25 mm, 1mm and 2 mm) with a voltage of 5 kV applied to the downstream electrode. The maximum electric field (near the right side of the downstream electrode) increases by about 60% when the tube thickness decreases from 1.0mm to 0.25mm. This is due to the effect of dielectric barrier which is directly proportional to the tube thickness. Therefore, the electric field along more particularly the tube axis necessarily diminishes when the dielectric barrier becomes more important. In the same time, the small electric field peak at the tube exit (due to the change of permittivity from quartz to air) varies in the inverse way. This small electric field peak decreases by about 64%when the tube thickness varies from 1.0mm to 0.25mm.This is a consequence of the simultaneous increase of the first high peak in order to maintain constant the total potential (integral of the electric field) which is equal to the potential applied to the powered electrode. The relative differences of the maximum electric field are obviously larger for a variation of the tube thickness from 2mm to 0.25mm as displayed in figure 4.

Figure 5 displays the downstream geometric field in the case of 3 values of the internal tube diameters (0.25 mm, 1mm and 2 mm) while the other tube parameters are not changed. As in the previous case when the tube thickness is parameterized, the variation of the tube diameter corresponds also to a variation of the dielectric barrier (not the part corresponding to the solid dielectric but to the gaseous one). This means that as expected when the tube diameter is decreased from for instance 2 mm (standard case) down to 0.5 mm, the maximum electric field is increased by about 38% while the shape of electric field near the tube exit showing a second but small peak changes in order to maintain constant the total applied potential at the powered electrode.

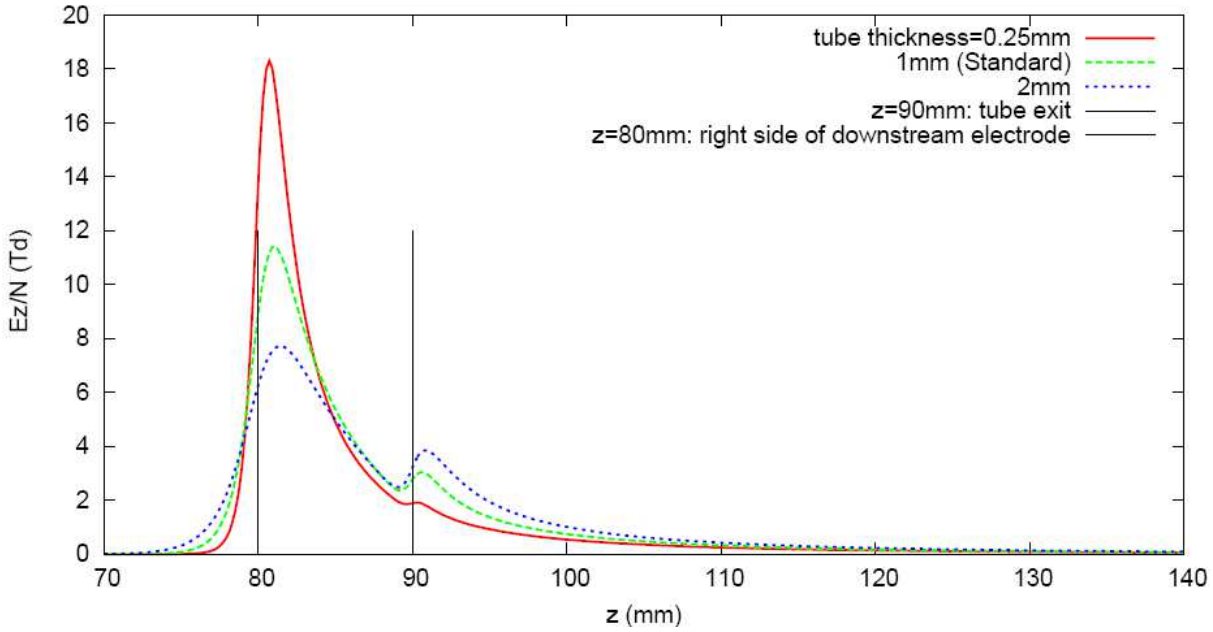

Figure 4: Axial variation of geometric electric field in the downstream side of the tube versus the tube thickness for 5 kV applied to downstream electrode.

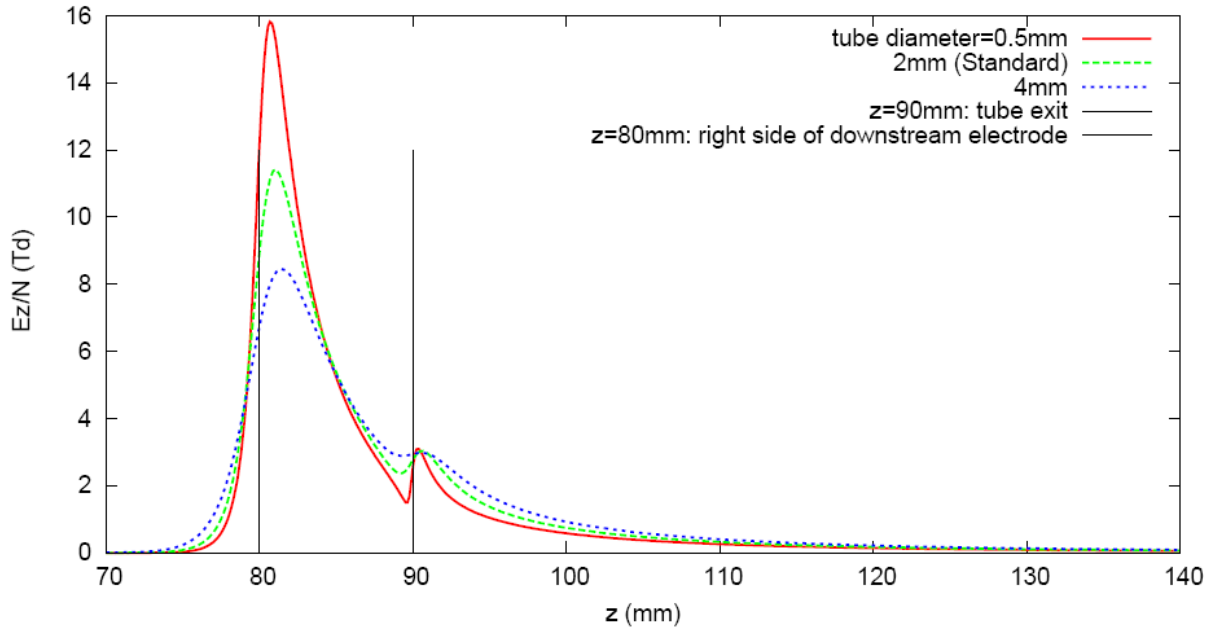

Figure 5: Axial variation of geometric electric field in the downstream side of the tube versus the tube diameter for 5 kV applied to downstream electrode.

Figure 6 displays the geometric field in the case of 3 values of the width of the downstream electrode (5 mm, 20mm and 30mm) while the other tube parameters remain unchanged. The magnitude of the maximum electric field increases by about 17% for each 10mm of the width diminution. In fact, if the electrode width is decreased, the charge density σon the electrode surface necessarily increases when the total charge number is maintained constant on this electrode. Therefore, the electric field near the downstream electrode has to increase to verifying the classical electrostatic relation of proportionality between the electric field ***E***near a conducting surface and the surface charge densityσ (***n*** being the unity vector perpendicular to the electrode surface).

$$\boldsymbol{E} = \frac{\sigma}{\varepsilon_0}\boldsymbol{n} \qquad (2)$$

As direct consequences:

- the electric field near the downstream electrode increases when the width of the downstream electrode decreases as it is shown in figure 6.
- The absolute value of electric field near the upstream electrode also increases when the width of the upstream electrode decreases.

In the case of a diminution of the upstream electrode width, the electric field close to the downstream electrode has to diminish (result not shown) in order to compensate the increase of the electric field near the upstream electrode. This compensation occurs to maintain constant the integral of the electric field along the z axis which is equal to the applied potential.

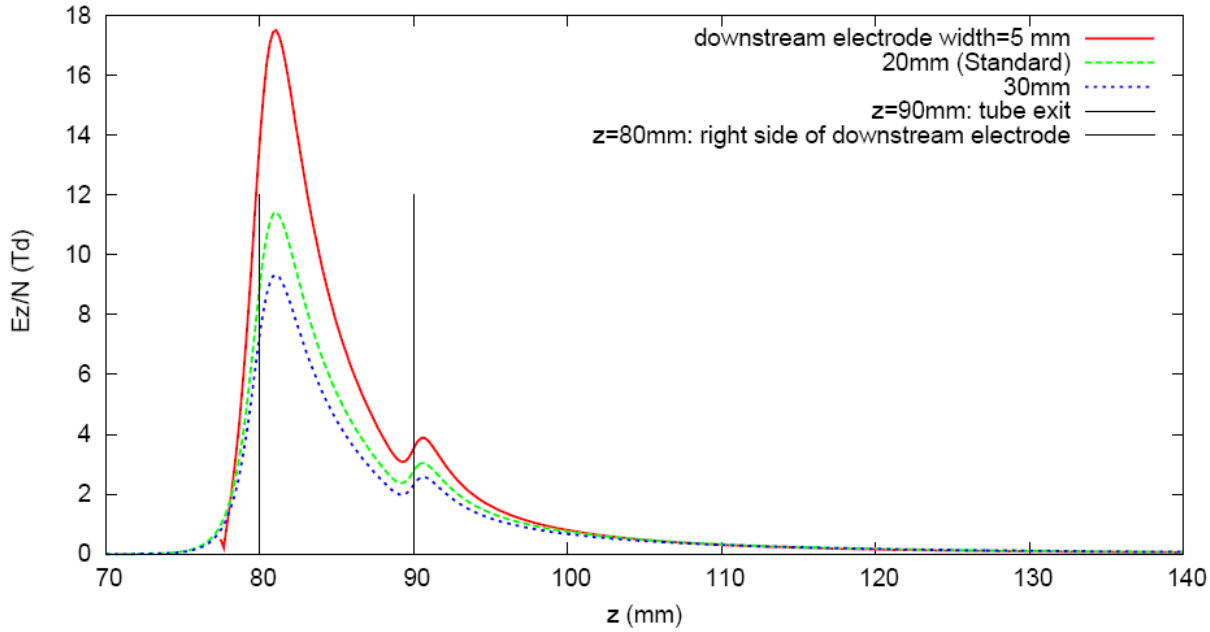

Figure 6: Axial variation of geometric electric field in the downstream side of the tube versus the downstream electrode width for 5 kV applied to downstream electrode.

To summarize, when the size of any electrode (upstream or downstream one) is decreased, the electric field near this electrode necessarily increases according to relation (2) between E and σ. If for instance, the size of downstream electrode is decreased (Fig. 6), the electric field near this electrode increases and in the same time the electric field near the other electrode (upstream one) decreases to maintain constant the integral of the total electric field.
Furthermore, from results not displayed, the variation of the inter-electrode distance *d* has only a small effect on the downstream electric field. In fact, the variation of *d* mainly affects the electric field magnitude between the electrodes (region III) which is inversely proportional to *d* in order to conserve the integral of the electric field between the electrodes. The consequence on the downstream electric (regions V and VI) is a small diminution of about 3% of the electric field maximum for 1 cm of increase of the inter-electrode distance.

Other electric field calculations have shown that the increase of the downstream electric field, requires thinner thickness of electrodes because as previously emphasized this contributes to decrease the total surface of the electrodes and therefore to increase the charge density. However,

the percentage of such an increase on the electric field is not really significant because it corresponds to about 10% electric field rise for anon negligible diminution (equal to 0.5mm) of the electrode thickness.

It is also interesting to observe the variation of the downstream electric field versus the variation of dielectric permittivity of the tube while keeping invariant the other tube parameters. As displayed in figure 7, the increase of the dielectric permittivity, from 2.9 for lex an up to 10 for alumina, leads to a diminution of about 25% of the maximum of the downstream electric field. In fact, as shown in equation (1), the electric field is inversely proportional to the dielectric permittivity and therefore decreases when the latter increases if the total charge remains constant.

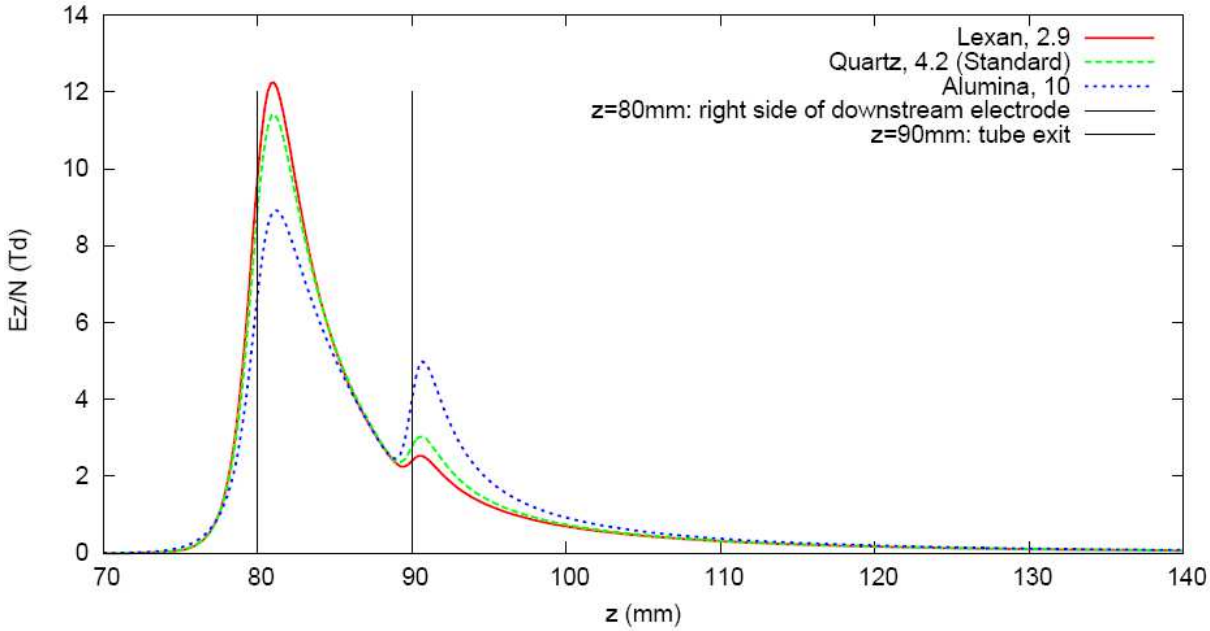

Figure7: Axial variation of geometric electric field in the downstream side of the tube versus the dielectric permittivity of the tube for 5 kV applied to downstream electrode.

Correlation between the maximum downstream electric field and plasma jet length

Two specific tube configurations have been selected to show that the magnitude of the electric field of region V in the downstream side (for $z \geq 70$ mm) has a direct effect on the properties of the ionization waves (or plasma bullets) ejected outside the tube in the downstream side (regions V and VI).

Figure 8 displays the geometric electric fields for two specific configurations corresponding to the sizes of the tube and the electrodes given in Table 1. The first configuration corresponds to the previous standard case and the second one to a configuration which is optimized to give a maximum of the downstream electric field higher than in the standard case. This optimized configuration corresponds to a judicious change of the sizes and positions of electrodes enabling us to increase the maximum of this electric field from about 11.5 Td to 20 Td i.e. an increase of more than 70%. In fact, we have not changed all the interesting parameters of the tube resulting from our previous parametric analysis. We have only changed the tube parameters easily changeable in our experimental setup such as the widths of upstream and downstream electrodes and the inter-electrode distance.

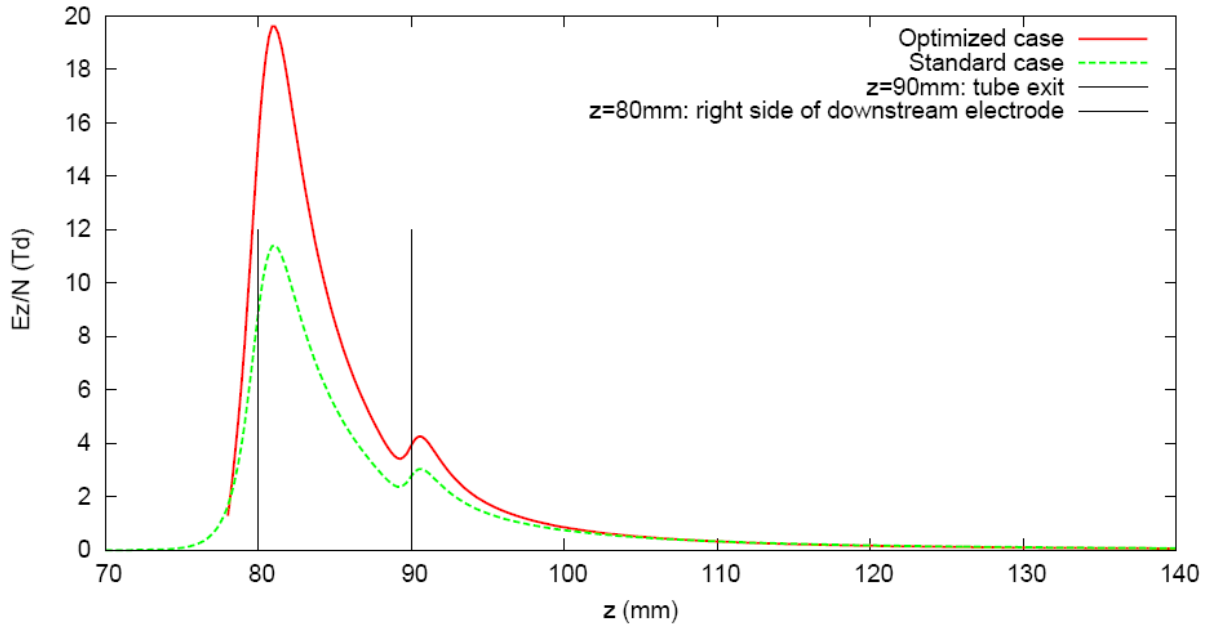

Figure 8: Comparison between the reference (or standard) and optimized cases for 5 kV applied to downstream electrode. NB: optimization is restricted only to the experimentally realizable cases that we had at our disposal

Unit=mm	ϕ_{int}	tk_{tube}	$w_{e,up}$	$w_{e,down}$	d	tk_e	L
standard	2	1	20	20	10	0.2	10
optmized	2	1	30	5	5	0.2	10

Table 1: Values of tube parameters in the standard and optimized cases using the same quartz tube (ε_r=4.2) for the experimental confirmation of the calculation trends. The tube and electrode parameters ϕ_{int}, tk_{tube}, $w_{e,up}$, , $w_{e,down}$, d , $tk_e$and L have already been defined in the caption of figure 1b.

Fluid modeling of ionization waves in standard and optimized tube sizes:

The consequences of the increase of the initial electric field on the ionization wave dynamics and the plasma jet length are first shown in figures 9 and 10 displaying the evolution of the variation of the electric field and electron density obtained from fluid model simulations of the dynamics of the ionization waves in the two tube configurations described in Table 2 (standard and optimized cases).

In order to simulate the development and the propagation of the ionization waves or plasma "bullets" launched in open air outside the dielectric tube, we used a fluid model based on the classical conservation equations of charged particles (electrons and ions) coupled to electric field equation (1) for charge space electric field calculations. It was already used for simulation of ionization wave dynamics in the same plasma jet setup and also in the case of streamer corona discharge dynamics. Details on the fluid model and the used numerical methods can be found elsewhere (see e.g. refs [36-37]).

Figures 9a and 9b show, at different instants of the ionization wave propagation in the case of a pulse width of 1660 ns, the space variation of the reduced electric field and the electron density along the quartz tube axis, starting from the right side of the downstream electrode (z=80mm) up to a distance z=120mm outside the tube (at 30mm from the tube exit). The considered gas flow velocity (15m/s) is identical to the experimental condition presented in section 3.3.2 (i.e. 3 liter/min). Figures 9a and 9b correspond to the case of the standard configuration while figures 10a and 10b display similar plots in the case of optimized configuration.

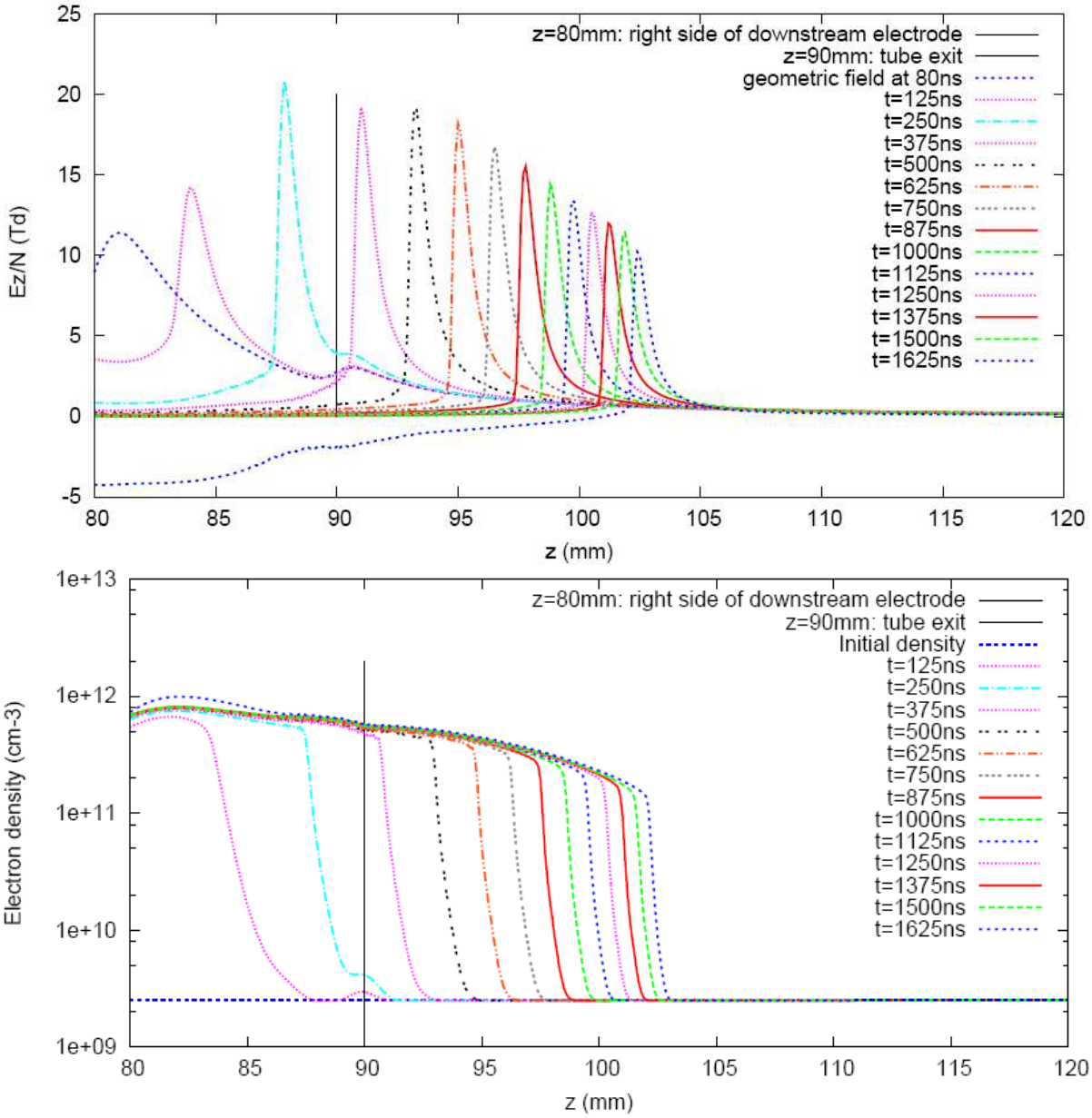

Figures 9: Electric field and electron density in the standard configuration in the case of a pulsed voltage with voltage amplitude V_0=5 kV and pulse width=1660ns including 80 ns of rise time and 80 ns of falling time.

Whatever the tube configuration, each curve (either of electron density or electric field) is plotted at every 125 ns, starting from the initial time corresponding to the beginning of the voltage pulse and covering the rise time (80 ns), the pulse width with a constant voltage of 5 kV (1500 ns) and the falling time (80ns) that leads to a total time of1660 ns. In the case of electron density for instance, the first curve (at t=0ns) corresponds to a constant density equal to the initial pre-ionized gas density.

Starting from the initial density, the electron avalanche increases mainly due to the stepwise ionization (as discussed in ref 36) until reaching a density level near 10^{12}cm^{-3}. Then the space variation of electron density displays a front shape with a maximum which slowly decreases during the ionization wave propagation. At each instant, the electron density maximum finishes by a sharp

decrease of a few decades down to the initial pre-ionization density. At a given instant, the position of this sharp density fall corresponds in fact to the front of the ionization wave.

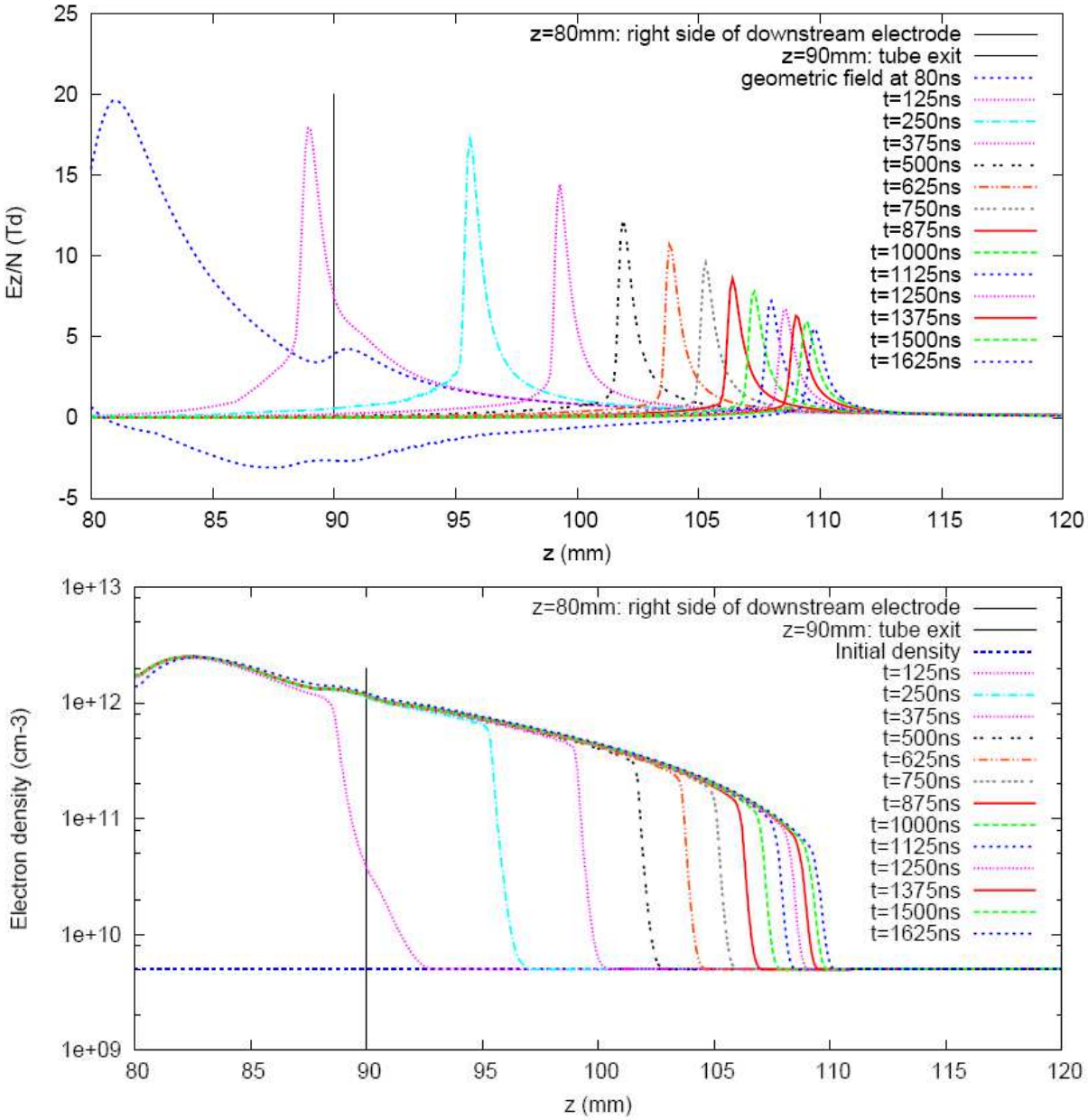

Figures 10: Electric field and electron density in the optimized configuration in the case of a pulsed voltage with voltage amplitude V_0=5 kV and pulse width=1660ns including 80 ns of rise time and 80 ns of falling time and 15 m/s for helium flow rate.

Such spatial variation of the electron density leads to a local increase of the space charge that in turn affects the magnitude and the shape of the initial geometric electric field. The space charge electric field displays a shape with a peak able to reach (during the first instants of the ionization wave propagation) about 20 Td in the case for instance of the standard configuration.

Then the front of the electron density and the peak of the space charge electric field move simultaneously along the tube axis with a variable propagation velocity that can reach a few hundreds of km/s. Table 2gives some ionization wave velocities reached at different instants of the plasma jet propagation in the standard and optimized cases.

Instant of propagation	125 ns	250 ns	375 ns	1625 ns
Standard configuration	670×10^3 m/s	32×10^3 m/s	24×10^3 m/s	9×10^3 m/s
Optimized configuration	710×10^3 m/s	56×10^3 m/s	32×10^3 m/s	9×10^3 m/s

Table 2: Calculated velocity of propagation of the ionization wave in the case of standard and optimized configuration of the tube.

The trends of the velocities of ionization waves are coherent with our previous simulations (ref 36)and also with the literature experimental observations (see e.g. ref 22).There is an acceleration of the ionization wave in the part of the tube between the right side of downstream electrode and the tube exit where helium gas flow is not yet mixed with ambient air. Then from the output of the tube, there is a gradual slowdown of the ionization wave concomitant with the helium dilution in air. This can be explained by the decrease of the ionization efficiency when the helium is progressively diluted in air during the propagation of the ionization wave. This leads to the gradual decrease of the electric field peak due to the decrease of the magnitude of space charges. The propagation of ionization waves lasts up to the end of the duration of the applied voltage pulse and starts following the same scenario during the next voltage pulse.

Table 2 shows that the propagation velocity is higher in the case of the optimized configuration and becomes similar for both configurations at the end of the propagation. Furthermore, figures 9 and 10 clearly show that the distance of the ionization wave propagation is the longest in the case of the optimized configuration (110 mm in the optimized tube configuration against 102 mm in the standard case). These figures also show that the electron density reaches higher magnitude for the optimized case, about 2×10^{12} cm^{-3} in the optimized case against about 10^{12} cm^{-3} in the region between the right side of downstream electrode and the tube exit.

These simulations of the dynamics of the ionization waves presented in this subsection give us a confirmation of the correlation between the magnitude of the initial geometric electric field of region V in the downstream side and the length of the plasma jet. Indeed, the higher initial downstream electric field in the optimized configuration leads to higher plasma characteristics (jet length, electron density, space charge electric field and current discharge).

Experimental confirmation of the effects of tube sizes on plasma jet characteristics:

In the following, the instantaneous discharge current and the plasma length have been measured in the two previous case of tube size (optimized and standard configurations) under the following electric and gas flow conditions:

- Maximum voltage applied to powered electrode: V_0=5 kV
- Pulse width: 1660 ns (including 80 ns for rising time and 80 ns for falling time)
- Pulse frequency: 9,69 kHz
- Helium gas flow rate: 3 liter/min

Recorded currents

Figure 11 displays the recorded current during the time evolution of the voltage pulse in the case of the two chosen tube configurations. As is previously emphasized in similar setups of plasma jet (see e.g. refs 16-17 and 23), there are two discharges for every voltage pulse. The sign of the recorded current is determined by the time derivative of the voltage pulse dV(t)/dt. The current sign is

positive when discharge is ignited during the rising time and negative when the second discharge is ignited during the falling time.

Whatever the tube configuration (optimized or standard one), during the rising time of the voltage pulse, there are two peaks in the recorded current which is positive (dV(t)/dt>0):a first peak(displacement current) followed by a second peak(discharge current). The dielectric barrier discharge current (second peak with a duration of about 150 ns) shows a classical shape characterized by an increase up to the arrival of the discharge at the powered electrode corresponding to the maximum current. This is followed by a relaxation stage dominated by the decay processes of charged particles. After the first discharge up to the beginning the second discharge occurring during the falling time of the pulse, a series of small oscillations (or rebounds)have been observed due to electromagnetic interferences in the impedance of the electrical circuit.

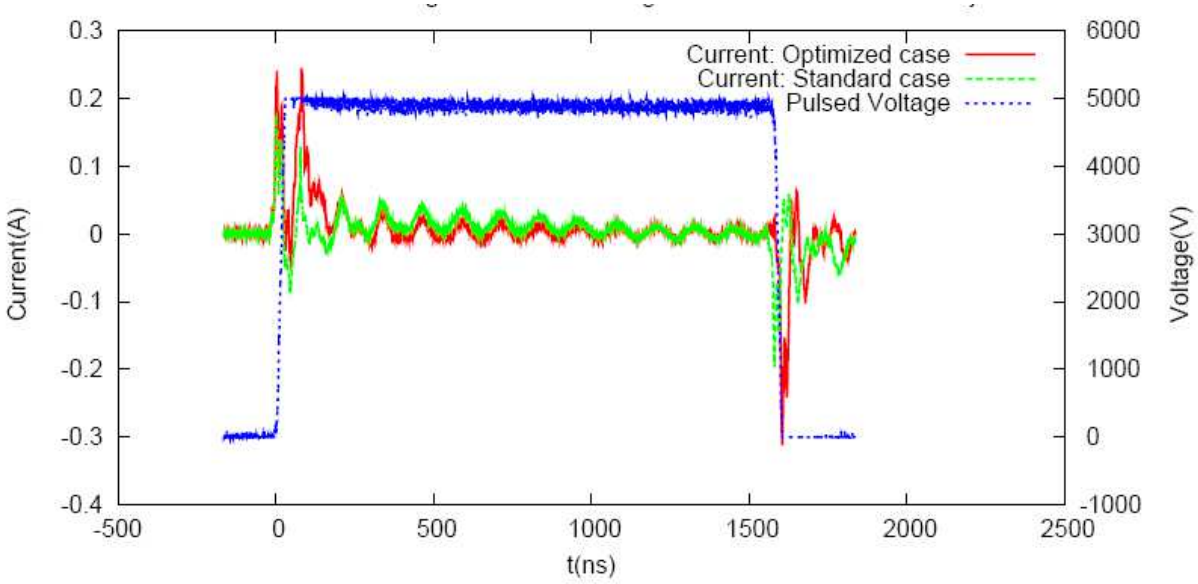

Figure 11:Instantaneous current (green and red lines) and applied pulsed voltage (blue line) to powered electrode versus time (voltage amplitude V_0=5 kV, pulse width=1660ns and repetition rate=9.69 kHz). NB: Near the rising edge, current includes displacement current (first peak) and discharge current (second peak) while during the falling edge, displacement and discharge currents are superposed

In the case of the second discharge occurring during the falling time of the pulse voltage, the recorded negative current (dV(t)/dt< 0) is the superposition of displacement and discharge currents. This second discharge evolves in the opposite direction to the first discharge (i.e. from the powered electrode towards the grounded one) with a current peak smaller than the first discharge current.

Furthermore, it is interesting to note that the direct comparison between the currents of the two considered tube configurations clearly show that positive current (or the first discharge current) and the negative current (or the second discharge current)are both higher in the case of the optimized tube configuration. The discharge current (either the positive or negative one) resulting from the optimized configuration is about twice higher than the current of the standard configuration.

Photos of the plasma jet

Last, the photos of the plasma jet in the two considered tube configurations (figure 12) clearly show that the length and the luminosity of the plasma jet are more important in the case of the optimized

tube configuration. The length of the plasma jet in the optimized configuration is more than twice longer than the case of standard configuration.
This result gives an additional confirmation of the correlation between the magnitude of the downstream geometric electric field and the plasma jet properties.

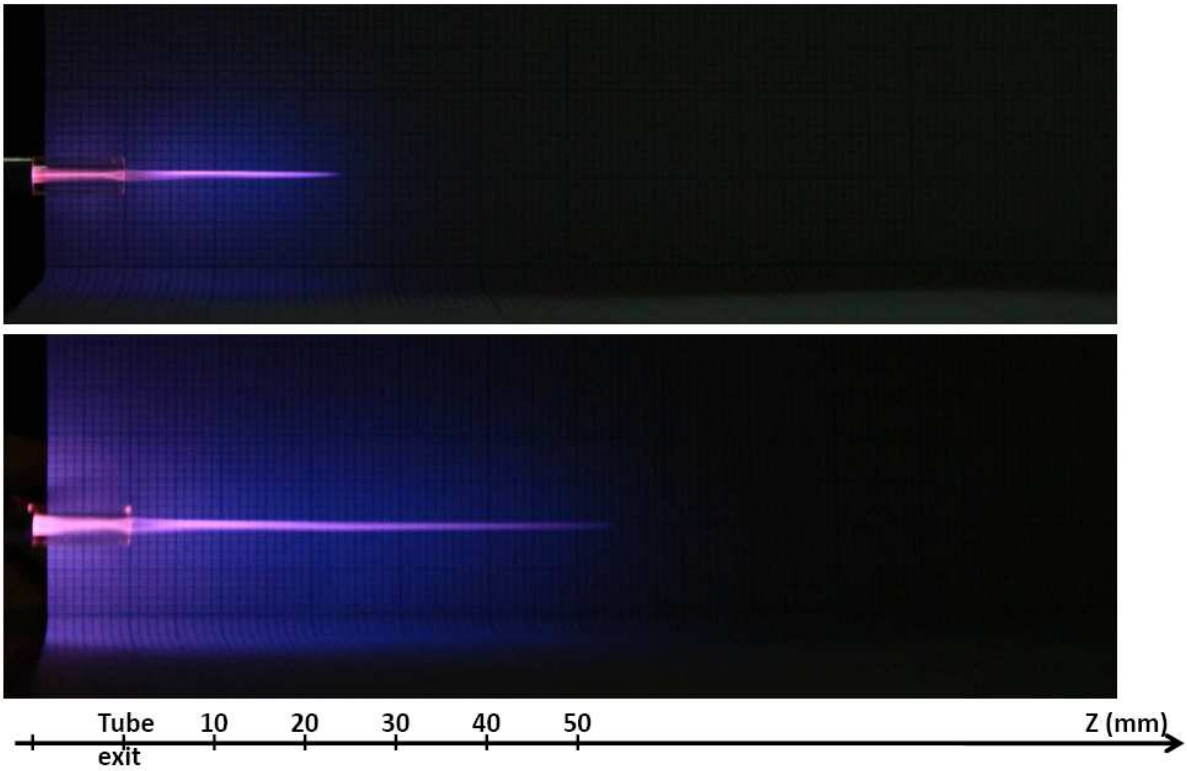

Figure 12: Photos of the plasma jet in the standard case (top view with jet length=25 mm) and optimized case (bottom view with jet length=55mm) for voltage magnitude V_0=5 kV, pulse width=1660ns repetition rate=9.69 kHz and helium flow rate of 3 liter/min.

CONCLUSION

A multi-parametric study of the tube and electrode sizes and the dielectric permittivity of the tube has been performed to analyze firstly their effect on the magnitude of the initial geometric downstream electric field. The magnitude of such electric field is determinant for the efficiency of the development and the propagation of the ionization wave dynamics in the case of the classical setup of dielectric barrier discharge using a quartz tube wrapped by two thin cylindrical external electrodes. The electrostatic calculations of the downstream electric field have shown that the highest magnitude of the initial geometric field can be obtained in the case of:

- The lowest dielectric permittivity
- The smallest downstream electrode width
- The largest upstream electrode width
- The thinnest electrode thickness
- The smallest inter-electrode distance
- The thinnest tube thickness
- The smallest tube diameter

Then, the effects of the magnitude of the downstream electric field on the dynamics of the plasma jet has been shown first from fluid modeling of the dynamics of ionizing waves (or bullets) and then from experimental measurements of the instantaneous discharge current and the plasma jet length in two chosen configurations (a standard and an optimized one) of tube and electrode sizes. In the

optimized tube configuration, we modified only the most easily changeable experimental parameters (i.e. the electrode sizes and positions) with the material that we have at our disposal. The experimental change of the other tube parameters (thickness, diameter and dielectric permittivity) will be considered in future works.

The trends of both fluid model simulations and experimental measurements have allowed the validation of the present multi-parametric approach. Fluid modeling and experimental results have clearly shown that the configuration corresponding to the highest magnitude of the downstream geometric electric field is the most favorable configuration for the most important ionization wave dynamics (jet length, electron density, space charge electric field, velocity of plasma bullets and discharge current).

Last, in order to have an idea on the improvement factor of the plasma jet characteristics in a theoretical (or ideal) choice of the tube and electrode parameters, we have simultaneously changed all the tube and electrode parameters studied in this work to get an optimal set of tube parameters. Figure 13 shows that the highest magnitude of the downstream electric field can be more than five times higher than the field of the standard configuration when using an optimal set of tube and electrode parameters given in caption of figure 13 under the same applied voltage to downstream powered electrode (5 kV).

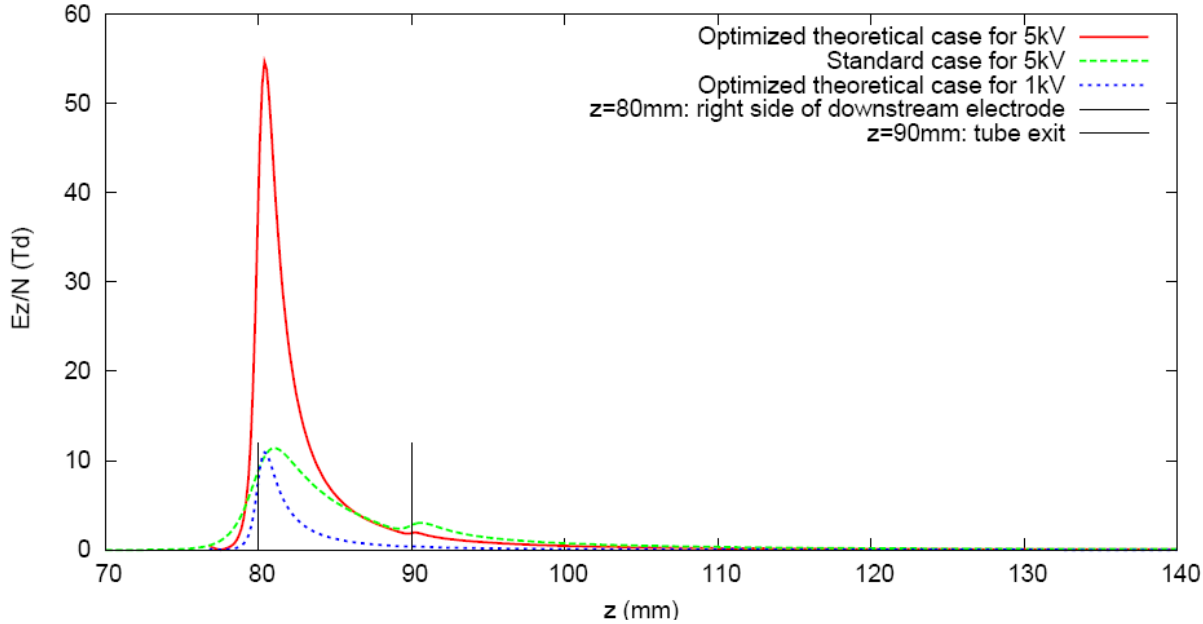

Figure 13: Comparison of downstream electric field between the standard case with 5 kV applied to downstream electrode and theoretical optimal configuration (dielectric permittivity = 2.9 (lexan or PVC), downstream electrode width=5mm, upstream electrode width=40mm, electrode thickness=0.2mm, inter-electrode distance=5mm, tube thickness=0.2mm and tube diameter=0.2mm.) for two applied voltages: 5kV and 1kV.

Therefore for such optimal theoretical configuration, it is expected to increase significantly the intensity and length of the present low temperature plasma jet in the limit of the saturation effects due to hydrodynamics phenomena. However, what seems better with this optimal configuration is to significantly decrease the magnitude of the applied voltage to get a low temperature plasma jet similar to the standard case. This is illustrated by figure 13 in the case of optimal configuration with an applied voltage of 1 kV that gives a maximum downstream electric field equivalent to the standard case using a voltage five times higher (5 kV). Therefore this theoretical optimal configuration is in principle able to design electric power supply using voltage about 5 times lower

than the standard voltage to generate the same low temperature plasma jet.

The future experimental confirmation of such a configuration using optimal tube and electrode parameters will be an interesting contribution targeting the reduction of the cost and the size of the electric power supply used for low temperature plasma jets.

REFERENCES

[1] M. Laroussi, IEEE Transactionson Plasma Science 30, 1409 (**2002**).

[2] A.MPointu, A. Ricard, B. Dodet, E. Odic, J. Larbre, and M. Ganciu, J. Phys. D 38, 1905 (**2005**).

[3] N. Abramzon, J.C. Joaquin, J. Bray, and G. Brelles-Marino, IEEE Transactions on Plasma Science 34, 1304 –1309 (**2006**).

[4] F Marchal, H Robert , N Merbahi, C Fontagné-Faucher, M Yousfi, C E Romain, O Eichwald, C Rondel, and B Gabriel, J. Phys. D: Appl. Phys. 45 , 345202 (**2012**).

[5]A.A. Meyer-Plath, K Schröder, B. Finke and A. Ohl, Vacuum71, 391–406 (**2003**).

[6] T. Desmet T, R. Morent , N. De Geyter, C. Leys, S. Schacht,and P. Dubruel, Biomacromolecules10, 2351-2378(**2009**).

[7] V.Samouillan, N. Merbahi, M. Yousfi, JP Gardou, F Delaunay, J Dandurand, and C Lacabanne, IEEE Transactions on Plasma Science 99, 1-9(**2012**).

[8] G. Fridman, G. Friedman, A. Gutsol, A.B. Shekhter, V.N. Vasilets, and A. Fridman, Plasma Process Polym 5, 503–33 (**2008**).

[9] E.Stoffels,Anton J. M. Roks, and E. Leo Deelman, Plasma Process. Polym.5, 599–605 (**2008**).

[10] G.E. Morfill, MG Kong, JL Zimmerman, New J. of Phys. 11, 115011(**2009**).

[11] G. Lloyd, G Friedman, S Jafri, G Schultz, AFridman, K Harding, Plasma Process. Polym.7, 194-211(**2010**).

[12] G.J. Kim, S. R Park., G. C Kim., and J.K Lee, Plasma Medecine 1, 45-55(**2010**).

[13] K.D.Wetman, K Dieter, E Kindel, T von Woedtke, M Hähnel, M Stieber, and R Brandenburg, Pure and Appl. Chem. 82, 1223-1237 (**2010**).

[14] M. G. Kong, B N Ganguly and R F Hicks, Plasma Sources Sci. Technol. 21, 030201 (**2012**).

[15] M. Teschke, J. Kedzierski, E. G. Finantu-Dinu, D. Korzec, and J. Engemann, IEEE Trans. Plasma Sci.33, 310 (**2005**).

[16] X. P. Lu, and M. Laroussi, J. Appl. Phys.100, 063302 (**2006**).

[17] B. L. Sands, B. N. Ganguly, and K. Tachibana, Appl. Phys. Lett.92, 151503 (**2008**).

[18] J. Shi, F. Zhong, J. Zhang, D. W. Liu, and M. G. Kong, Phys. Plasmas15, 013504 (**2008**).

[19] X. Lu,Q. Xiong, Z. Xiong, J. Hu, F. Zhou, W. Gong, Y. Xian, C. Zou, Z. Tang, Z. Jiang, and Y. Pan, J. Appl. Phys.105, 043304 (**2009**).

[20] Q. Xiong, X. Lu, K. Ostrikov, Z. Xiong, Y. Xian, F. Zhou, C. Zou, J. Hu, W. Gong, and Z. Jiang, Physics of Plasmas 16, 043505 (**2009**).

[21] N. Jiang, A. Ji, and Z. Cao, J. Appl Phys.106, 013308 (**2009**).

[22] N Mericam-Bourdet, M Laroussi, A Begum and E Karakas, J. Phys. D: Appl. Phys. 42 055207 (**2009**).

[23] J. Jarrige, M. Laroussi and E. Karakas, Plasma Sources Sci. Technol. 19, 065005 (**2010**).

[24] K. Urabe, T. Morita, K. Tachibanaand B N Ganguly, J. Phys. D: Appl. Phys. 43, 095201 (**2010**).

[25] E Karakas, M Kokluand M Laroussi, J. Phys. D: Appl. Phys.43, 155202,(**2010**).

[26] K. Urabe, H. Motomura, O. Sakai and K. Tachibana J. Phys. D: Appl. Phys. 44, 042001 (**2011**).

[27] T.Gerling, A V Nastuta, R Bussiahn, E Kindeland K.D.Weltmann, Plasma Sources Sci. Technol. 21, 034012 (**2012**).

[28] Qing Li,Wen-Chao Zhu, Xi-Ming Zhu and Yi-Kang Pu, J. Phys. D: Appl. Phys. 43, 382001 (**2010**).

[29] B. L. Sands, S. K Huang, J. W Speltz, M. A Niekamp, J. B Schmidtand B. N Ganguly ,Plasma Sources Sci. Technol. 21, 034009 (**2012**)

[30] Z. Xiong, X. Lu, Y. Xian, Z. Jiang and Y. Pan J. Appl. Phys.108, 103303 (**2010**).

[31] J LWalsh, P Olszewski and J W Bradley, Plasma Sources Sci. Technol. 21, 034007 (**2012**).

[32] N. Jiang, A. Ji, and Z. Caoa, J Appl.Phys.108, 033302 (**2010**).

[33] K. Urabe, Y. Ito, O. Sakai, and K. Tachibana, Jpn. J. Appl. Phys. 49, 106001 (**2010**).

[33]G V Naidis, J. Phys. D: Appl. Phys. 43, 402001 (**2010**).

[34] Y. Sakiyama, D. B. Graves, J. Jarrige and M. LaroussiAppl. PhysLett. 96, 041501 (**2010**).

[35] D. Breden, K. Miki, and L. L. Raja, Appl. PhysLett. 99, 111501 (**2011**).

[36] M Yousfi, O Eichwald, N Merbahi and N Jomaa, Plasma Sources Sci. Technol. 21 045003 (**2012**).

[37] O. Eichwald, H. Bensaad, O. Ducasse and M. Yousfi1, J. Phys. D: Appl. Phys. 45, 385203 (**2012**).